ELSEVIER

Catalysis Today 78 (2003) 411–417

CATALYSIS TODAY

www.elsevier.com/locate/cattod

Hyperfine interactions studies on Pt–In/Nb_2O_5 catalysts

Fabio B. Passos [a,*], Ingridy S. Lopes [a], Paulo R.J. Silva [b], Henrique Saitovitch [b]

[a] *Departamento de Engenharia Quimica, Universidade Federal Fluminense, em, Rua Passos da Patria, 156, 24210-240 Niterói, RJ, Brazil*

[b] *Centro Brasileiro de Pesquisas Físicas, MCT, Rua Dr. Xavier Sigaud, 150, 22290-180 Rio de Janeiro, RJ, Brazil*

Abstract

Pt–In/Nb_2O_5 catalysts were investigated using temperature-programmed reduction (TPR) and time differential perturbed angular correlation (TDPAC) experiments. The results indicated the presence of In–O surface complexes for low loading In/Nb_2O_5 and Pt–In/Nb_2O_5 catalysts after calcination. These complexes did not form a In_2O_3 crystalline phase. After reduction of the Pt–In/Al_2O_3 catalyst, In is present in different states. A fraction of In atoms is bonded to niobia surface, as a surface complex that does not show crystalline structure similar to bulk In_2O_3. Other fraction of In atoms interacts with platinum, in the form of an alloy, in locations that present trigonal symmetry.

Keywords: Angular correlation; Niobia; Platinum

1. Introduction

Niobia supported platinum catalysts have been investigated as alternative catalysts for hydrocarbon conversion [1–3]. After reduction at 773 K, platinum particles are decorated by partially reduced niobia species, with the creation of new interfacial sites [4]. This catalytic system displayed a higher selectivity towards the formation of olefins in the *n*-heptane dehydrogenation as compared to conventional dehydrogenation catalysts. However, they were not stable [1]. The dehydrogenation of paraffins is commercially carried out using an alumina supported platinum catalyst, containing indium as a promoter [5]. Indium is able to dilute the platinum particles in these catalysts and improve the selectivity, stability and activity in *n*-heptane dehydrogenation [6]. Thus, the addition of In could be an alternative to improve the stability of Pt/Nb_2O_5 catalysts.

In this work, we report the characterization of Pt–In/Nb_2O_5 using temperature-programmed reduction (TPR) and time differential perturbed angular correlation (TDPAC).

TDPAC is a nuclear spectroscopy which enables us to characterize materials in an atomic scale through hyperfine interactions (HIs) studies, here represented by the interactions between the nuclear electric quadrupole moment of a suitable radioactive probe-isotope and the electric field gradients originated from its neighborhood. Characteristic measured parameters, obtained via detection of emitted γ's originated from the nuclear cascade of the probe-isotope, are *nuclear quadrupole frequency interactions* and *asymmetry* parameters. The properties of materials are essentially determined by their microstructure. TDPAC spectroscopy, besides allowing to detect small amounts of lattice structural phases hardly detected by X-ray diffraction, is showing to be a valuable tool,

* Corresponding author. Fax: +55-21-2717-4446.
E-mail address: fbpassos@engenharia.uff.br (F.B. Passos).

0920-5861/02/$ – see front matter
PII: S0920-5861(02)00308-5

via HI studies, to characterize the local environment of impurities in solids, because of the nature of the information they display. Although the application of this technique in materials characterization have been used intensively and systematically, only recently it has been applied to catalytic systems [7]. In the case of Pt–In/Al_2O_3 catalysts, TDPAC was instrumental to further characterize the interaction between Pt and In and show that the surface composition is non-uniform [8,9].

2. Angular correlation

In this section, we make a brief review on the theory of TDPAC in such way to help the understanding of the experimental results on catalysts. Comprehensive descriptions of the TDPAC theory can be found elsewhere [10,11].

The intensity distribution of γ-rays emitted from excited states of nuclei belonging to a nucleae ensemble is dependent upon the angle the emission directions have relatively the nuclear states spin orientations. Such behavior is usually hidden because as far as in a excited nucleae ensemble all the spin orientations are equally probable, the detection of the emitted γ-rays displays an isotropic intensity pattern, always if we assume the detection occurs at same distances around the emitting sample. The anisotropic intensity pattern which is known to exist would appear if it would be possible to detect only γ-rays originated from unidirectional aligned spin sub-ensemble belonging to the total nucleae ensemble.

Such unidirectional spin aligned sub-ensemble can be "isolated" by detecting, in a well defined direction, the γ-rays originated from the first excited state (γ_1) of a decaying nuclear cascade. If they are detected in that direction they must have been originated from a unidirectional aligned spin orientation sub-ensemble. The next step is to detect the γ-rays originated from the intermediate state of that cascade (γ_2); because of the requirement for the total angular momentum conservation (nuclear excited state spin plus γ-ray spin) they will be emitted accordingly to the angles defined by both the γ-rays. In order to make sure that both γ-rays originated in the same nucleus, in such a way keeping the coherence of the experimental information, an electronic coincidence circuit, starting operation upon the arrival of a "start pulse1" (connected to γ_1-ray), only delivers a "counting pulse" if during a "coincidence time" previously adjusted (always in a scale of nanosecond) it arrives a "stop pulse2" (connected to γ_2-ray). In this way, with the observation of γ_1-rays, a unidirectionally spin oriented sub-ensemble of nuclei is selected; by measuring their coincidence with γ_2-rays, only those γ_2-rays which are emitted by this same sub-ensemble are detected. This effect of angular preferred direction emission is known as angular correlation (AC). It is characterized by the nuclear parameter anisotropy and here recorded as angle dependent γ_1–γ_2 coincidence counting rates. In cases where the intermediate excited state of the nuclear cascade (which de-excitation originates the γ_2-ray) has an extended lifetime compared to the so-called "resolution time" (usually ≈1.5–2.0 ns) of the experimental setup, the coincidence counting rate, fixed in a definite angle between both detectors, displays an exponential function in time related to the lifetime of the intermediate nuclear state decay. This is the case of the isotope-probe $^{111}In \rightarrow {}^{111}Cd$ used in our experiments, where ^{111}In is the isotope-probe introduced in the material and ^{111}Cd its decay-isotope on which decaying nuclear cascade the measurements are performed. This modality is known as time differential angular correlation (TDAC). When extra nuclear fields—electric field gradients and/or magnetic fields—originated from charges in the vicinity of the nuclear-probes introduced in the material under research are present they may interact (the so called HI) with the respective nuclear parameters—electric quadrupole moments and/or magnetic dipole moments—these oriented spin nuclei may reorient during the finite lifetime of the intermediate quantum level (this reorientation can be described semiclassically as the precession of the nuclear spin vector); and as far as a nucleus processes during the lifetime of its intermediate quantum level, the probability of emitting the second γ-ray in the direction of the second detector changes, because the nucleus is no longer oriented in the initial direction. This subtle effect is said to "perturb" the AC; and then we are dealing with TDPAC, which may be expressed as:

$$W(\theta, t) = \exp\left(-\frac{t}{\tau_N}\right)[1 + A_{22}G_{22}(t) \cdot P_2(\cos\theta)] \quad (1)$$

where A_{22} is the anisotropy of the γ_1–γ_2 isotope-probe nuclear cascade, $P_2(\cos\theta)$ the Legendre polynomial, G_{22} the time dependent perturbation factor, contains all the relevant information concerned with the perturbations, and τ_N lifetime of the intermediate level of the TDPAC nuclear cascade.

Experimentally the time distribution $W(\theta, t)$ is given by the coincidence counting rate between γ_1 and γ_2 as a function of the intermediate quantum level lifetime, and of a particular angle θ between the detectors of the two γ-rays. The EFG, second derivative of the electric potential at the probe-isotope, is a traceless tensor which, in a principal axis coordinate system, is completely characterized by the two parameters: V_{zz} (chosen as the largest EFG component: $|V_{zz}| \geq |V_{yy}| \geq |V_{xx}|$), determined by the nuclear electric quadrupole frequency $\nu_Q\,(\mathrm{Hz}) = eQV_{zz}/h$ where Q is the nuclear electric quadrupole moment, e the electron charge, h the Planck's constant and the asymmetry coefficient $\eta = (V_{xx} - V_{yy})/V_{zz}$ ($0 \leq \eta \leq 1$) reflects a local deviation from axial symmetry ($\eta = 0$).

For nuclear electric quadrupole static interactions in a polycrystalline sample, without texture or some other inner crystal orientation, the most general perturbation factor can be written as a superposition of several oscillatory components:

$$G_{22}(t) = \sigma_{20}(\eta, \nu_Q) + \sum \sigma_{2n}(\eta, \nu_Q) e - F(\delta, w_n, t) e - 1/2\tau_R^2\omega_n^2 \cos(\omega_n t) \quad (2)$$

where $\omega_n = g_n(\eta)\nu_Q$ is the transition frequencies between the magnetic sub-levels of the spin's probe-isotope intermediate nuclear state, δ the ω_n frequencies relative distribution width (usually normalized to 1.0), τ_R the time resolution of the measurements setup, and σ_{2n} the expansion coefficients:

$$F(\delta, \omega_n, t) = \begin{cases} \delta\omega_n t & \text{(Lorentzian distribution)} \\ \frac{1}{2}(\delta\omega_n t)^2 & \text{(Gaussian distribution)} \end{cases}$$

In the case of electric field gradient fluctuations, in a time scale comparable to the experimental lifetime of the probe-isotope intermediate nuclear state cascade and setup time resolution, the perturbation factor may be expressed as $G_{22}(t) = \exp(-\lambda_2 t)$.

3. Experimental

3.1. Catalyst preparation

Niobia (BET area = 65 m^2/g) was obtained by calcination of niobic acid (CBMM HY340) for 2 h.

Pt/Nb_2O_5 was prepared by incipient wetness using an aqueous solution of H_2PtCl_6 (Merck). After impregnation, the sample was dried at 373 K for 24 h followed by calcination at 773 K for 2 h.

$Pt–In/Nb_2O_5$ catalysts were prepared by impregnating the calcined Pt/Nb_2O_5 catalyst with an aqueous solution of $In(NO_3)_3$ (Aldrich) followed by drying at 373 K and calcination at 773 K.

3.2. Temperature-programmed reduction

TPR measurements were carried out in a microreactor coupled to a quadrupole mass spectrometer (Balzers, Omnistar). The samples (300 mg) were dehydrated at 423 K for 30 min in a He flow prior to reduction. After cooling to room temperature (RT), a mixture of 5% H_2 in Ar flowed through the sample at 30 cm^3/min, raising the temperature at a heating rate of 10 K/min up to 773 K.

3.3. Time differential angular correlation

The carrier free ^{111}In TDPAC suitable probe-isotope was added to all the samples by diffusing ^{111}In (10–4 at.%) to the $In(NO_3)$ impregnation solution; so the probe-isotope would go to the same positions as In atoms. The samples were placed in an experimental setup that allowed to perform in situ TDPAC experiments as well as their treatment. The samples were reduced at 773 K for 2 h under a flow of H_2 (30 cm^3/min).

In the present work the measurements were performed on the ^{111}Cd (172–247 keV) nuclear cascade, $\tau_n = 122$ ns [12]. The TDPAC experiments were carried out with a "fast–slow" [13] coincidence timing electronic four detector setup with BaF_2 scintillation crystals mounted on photomultipliers in a plane, at 90° intervals. The setup resolution time τ_R-uncertainty related to the time difference between, in principle, two simultaneous events was ≈1.5 ns and an electronic router allowed to store 12 simultaneous coincidence

spectra, each of them a superposition of the perturbation onto the exponential decay of the intermediate level of the ^{111}Cd nuclear cascade convoluted with the setup's resolution time curve (Gaussian). The spectra were then combined to obtain the intensity ratios (the exponential terms and counting efficiencies of the detectors cancel through the quotient):

$$R(t) = 2\frac{\sqrt[8]{\prod_{i=1}^{8} W_i(90,t)} - \sqrt[4]{\prod_{i=1}^{4} W_i(180,t)}}{2\sqrt[8]{\prod_{i=1}^{8} W_i(90,t)} + \sqrt[4]{\prod_{i=1}^{4} W_i(180,t)}} \quad (3)$$

where $W_i(\theta, t)$ is the number of coincidences for a specific detectors configuration, angle and time. The two measurement angles, 90° and 180°, are chosen in order to maximize the $R(t)$ amplitude oscillations, as far as their Legendre polynomials difference reaches a maximum value. The $R(t)$ were fitted by means of a nonlinear least square program based on the parameters of the $A_2G_{22}(t)$ function.

4. Results and discussion

4.1. Temperature-programmed reduction

TPR profiles of the catalysts are presented in Fig. 1. The profile of Pt/Nb_2O_5 presented reduction peaks at RT and 355 K that correspond to PtO_2 reduction [14]. A peak at 500 K was also observed and it is usually ascribed to an oxychloroplatinum surface complex [15]. The broad peak centered at 648 K is related to partial reduction of the support [4].

$Pt–In/Nb_2O_5$ presented similar spectra to Pt/Nb_2O_5 with the reduction of In taking place at lower temperatures than in the case of In/Nb_2O_5. The amount of H_2 consumed during TPR experiments is listed in Table 1. The difference between H_2 uptakes during TPR of 1% Pt–0.7% In/Nb_2O_5 and of 1% Pt/Nb_2O_5 indicates that approximately 50% of In is in a zero-valent state. This is in the same range as observed previously for $Pt–In/Al_2O_3$ catalysts [6].

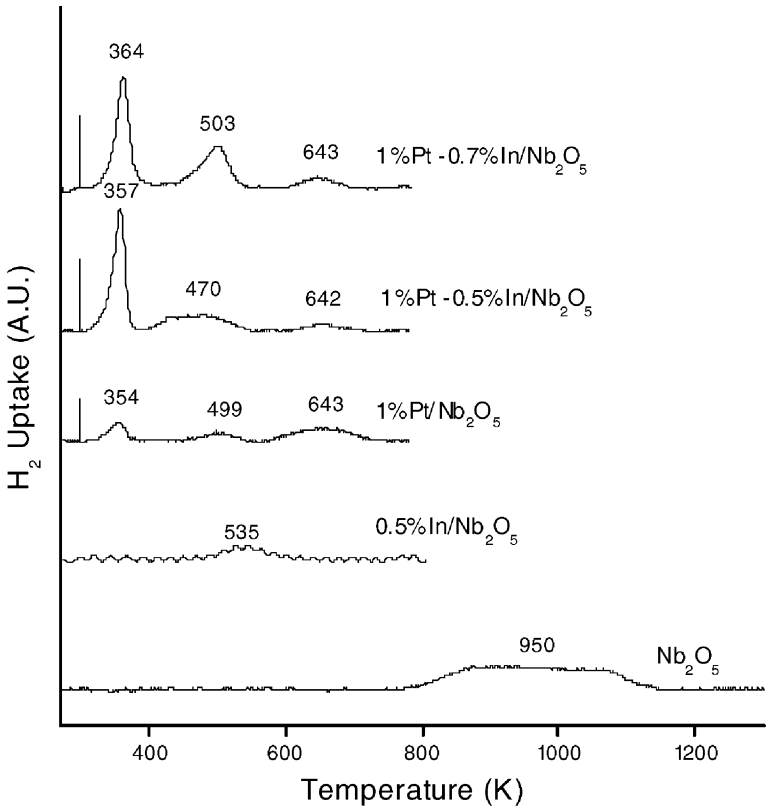

Fig. 1. TPR of $Pt–In/Nb_2O_5$.

Table 1
TPR results

Catalyst	Final reduction temperature (K)	H_2 uptake (μmol/g cat)
Nb_2O_5	1273	41.6
0.5% In/Nb_2O_5	773	11.6
1% Pt/Nb_2O_5	773	64.3
1% Pt–0.5% In/Nb_2O_5	773	104.5
1% Pt–0.7% In//Nb_2O_5	773	110.3

4.2. Time differential perturbed angular correlation

TDPAC results are displayed in Fig. 2, while Table 2 shows the hyperfine parameters adjusted from the experiments. After calcination, the 1% Pt/Nb_2O_5 ^{111}In doped catalyst showed a frequency distribution pattern (Fig. 2a), indicating the atoms of ^{111}In were not located in translational repetitive crystalline lattice sites. A distribution of frequencies informs on the existence of species with different degrees of coordination. The parameter δ in Table 2 shows this distribution. As the samples were prepared by impregnation, $^{111}In^{3+}$ was adsorbed on the niobia surface, and the observed frequency distribution indicates the formation of In–O bonds in a superficial complex, without the formation of bulk In_2O_3. Bulk In_2O_3 structure is trigonal, each In atom being coordinated by six oxygen atoms so that two characteristic sites are observed by TDPAC [16]. These results are consistent to temperature-programmed results that showed the presence of a surface complex of indium and oxygen after the calcination step for In/Nb_2O_5 catalysts. Similar frequency distribution results were previously obtained for Pt/Al_2O_3 catalysts [8,9] and for oxidized In implanted Pt [17]. After reduction of the above 1% Pt/Nb_2O_5 catalyst, at 773 K, the TDPAC displayed a spectrum (Fig. 2b) typical of a Pt–In alloy with trigonal symmetry [18]. This is a strong indication of the tendency of alloy formation in Pt–In/Nb_2O_5, and it is consistent with previous results for Pt–Sn/Nb_2O_5 [1] where the formation of Pt–Sn alloys was observed. In the case of Pt/Al_2O_3 catalysts, an interaction of Pt and In was also noted [8,9], but there was not the formation of regular Pt–In alloy structures. Thus, the interaction between active metal and promoter is higher when Nb_2O_5 is used as support. The reduced Pt–Nb_2O_5 (diffused ^{111}In impurity) displayed similar spectra at RT and 773 K (Fig. 2b and c), indicating same structures at both temperatures. The exposure of the Pt/Nb_2O_5 sample to air caused the oxidation of the alloy as well as the formation of In–O bonds that were not in a regular crystalline-like structure (Fig. 2d) as a frequency distribution was observed. The Pt–In alloy was formed again after repeating the reduction treatment (Fig. 2e).

For all the samples, after reduction at 773 K a relaxation pattern was also observed (parameter λ in Table 2). This is related to a mobility of the neighborhood of the probe-isotope in the samples [9].

Table 2
HIs parameters adjusted from the experiments[a]

T(K)	ν_Q (MHz)	η	f^I	δ	f^{II}	λ (s^{-1})
1% Pt/Nb_2O_5						
RT (calcined, Fig. 2a)	155.6 (5.4)	0	1	0.6 (0.03)	0	
773/H_2 (Fig. 2b)	247.6 (2.8)	0.27 (0.02)	0.88 (0.05)	0.22 (0.01)	0.12 (0.01)	14.3 (3.8)
RT/H_2 (Fig. 2c)	254.8 (4.0)	0.22 (0.03)	0.86 (0.05)	0.28 (0.02)	0.14 (0.01)	9.4 (2.8)
RT/air (Fig. 2d)	154.1 (5.4)	0		0.67		
773/H_2 (after air, Fig. 2e)	247.3 (3.5)	0.24 (0.03)	0.78	0.24 (0.02)	0.22 (0.01)	18.5 (2.4)
1% In/Nb_2O_5						
RT (calcined, Fig. 2f)	192.7 (5.2)	0	1	0.6 (0.03)	0	
773/H_2 (Fig. 2g)	232.8 (3.0)	0	0.60	0.79 (0.03)	0.40	5.5
1% Pt/1% In/Nb_2O_5						
RT (calcined, Fig. 2h)	142.9 (5.9)	0	1	0.92	0	
773/H_2 (Fig. 2i)	209.0 (13.6)	0	0.81	0.63	0.19 (0.01)	15.0 (2.0)
RT/H_2 (Fig. 2j)	219.3 (13.7)	0	0.83	0.63	0.17 (0.01)	14.6 (2.2)

[a] η_Q: nuclear electric quadrupole interaction frequency; η: asymmetry parameter; δ: distribution of nuclear electric quadrupole interaction frequency; λ: relaxation parameter; f: fraction of sites.

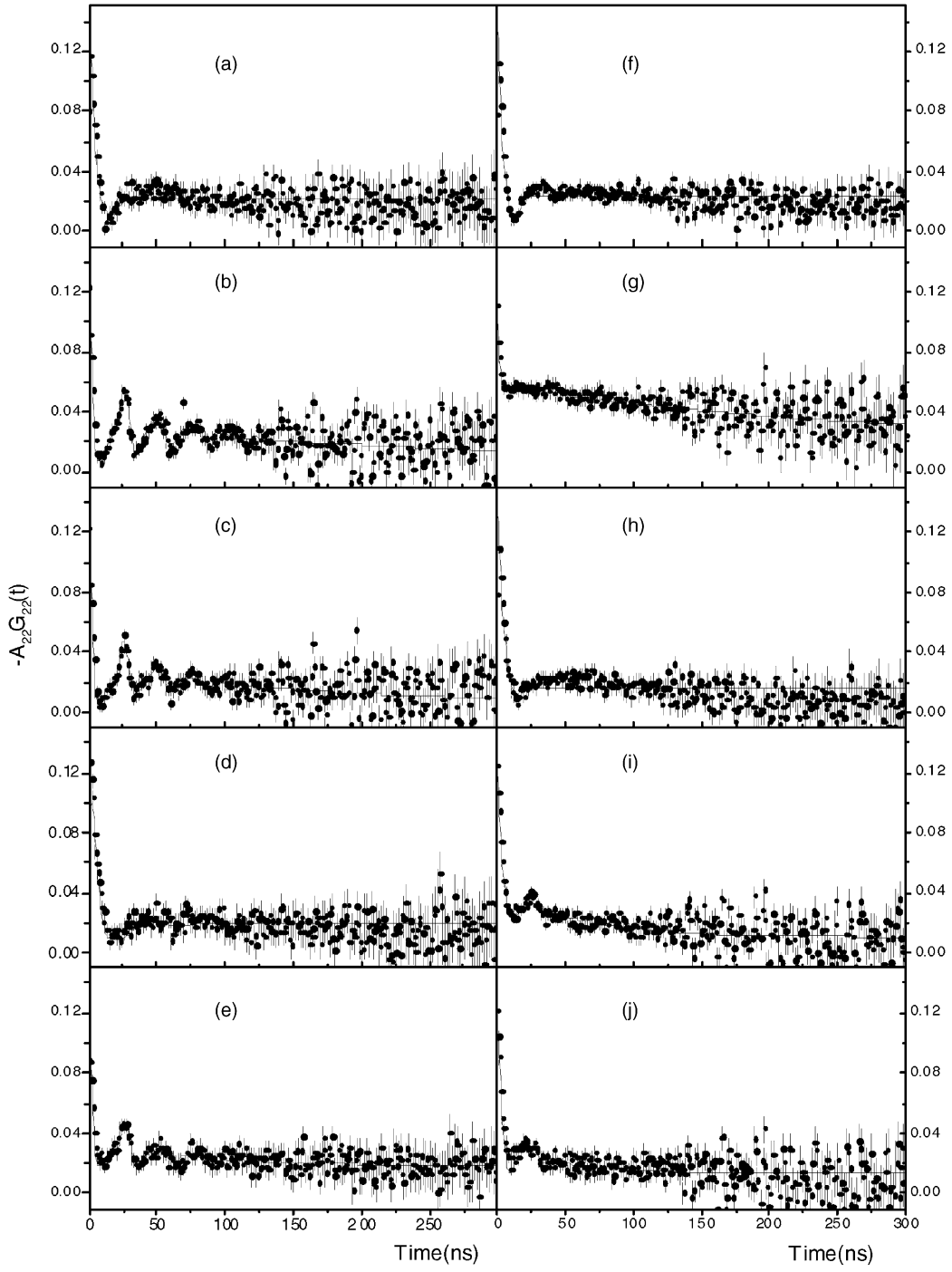

Fig. 2. TDPAC measured spectra. 1% Pt/Nb_2O_5: (a) calcined, measurement at RT; (b) after reduction at 773 K, measurement at 773 K; (c) reduced, measurement at RT; (d) after air exposure at RT, measurement at RT; (e) after new reduction, measurement at 773 K. 1% In/Nb_2O_5: (f) calcined, measurement at RT; (g) after reduction at 773 K, measurement at 773 K. 1% Pt/1% In//Nb_2O_5: (h) calcined; (i) after reduction, at 500 °C; (j) reduced, measurement at RT.

The 1% In/Nb_2O_5 system, after calcination, presented a frequency distribution pattern (Fig. 2f) (In_2O_3 pattern absent). Our recent work demonstrated in the case of Al_2O_3 supported catalysts the formation of In_2O_3 structure only for high In contents of the sample [9]. For low In contents, In–O bonds are formed but are well dispersed and thus they are not arranged in a regular crystalline-like structure. After reduction we could not observe the formation of a In^0 structure, as there was again the display of a frequency distribution pattern. This finding is consistent to the TPR experiments, that showed there was only a fraction of In atoms was reduced. Thus, the combination of some In^0 formation and the remaining In–O irregular structures lead to a frequency distribution pattern.

For the 1% Pt–1% In/Nb_2O_5 catalyst, after calcination, a frequency distribution pattern concerned to the In–O bonds was obtained (Fig. 2h). The reduction of this sample lead to a pattern (Fig. 2i) for which the main frequency observed (ν_Q) is similar to the value of Pt–In alloy but there is still a high frequency distribution. This can be interpreted as the combination of the formation of Pt–In alloy and the formation of In–O bonds. This picture also agrees with the TPR experiments that showed that around 50% of the In atoms is in a zero-valent state, i.e., the surface is multicomponent.

5. Conclusions

The TDPAC results indicated the presence of In–O complexes for low loading In/Nb_2O_5 and Pt–In/Nb_2O_5 catalysts after calcination. These complexes do not form In_2O_3 crystalline phase. After reduction, for Pt–In/Al_2O_3, it was evidenced In was present in different states. A fraction of In atoms is bonded to niobia surface, as a surface complex that does not show crystalline structure similar to bulk In_2O_3. Other fraction of In atoms interacts with platinum, in the form of an alloy, in locations that present trigonal symmetry.

References

[1] D.A.G. Aranda, F.B. Passos, F.B. Noronha, F.B. Passos, M. Schmal, Catal. Today 16 (1993) 397.
[2] D.A.G. Aranda, A.L.D. Ramos, F.B. Passos, M. Schmal, Catal. Today 28 (1996) 119.
[3] F.B. Passos, D.A.G. Aranda, R.R. Soares, M. Schmal, Catal. Today 43 (1998) 3.
[4] D.A.G. Aranda, F.B. Passos, F.B. Noronha, F.B. Passos, M. Schmal, Appl. Catal. 100 (1993) 77.
[5] H. Abrevaya, T. Imai, US Patent 4 608 360 (1986).
[6] F.B. Passos, D.A.G. Aranda, M. Schmal, J. Catal. 178 (1998) 478.
[7] T. Butz, C. Vogdt, A. Lerf, H. Knözinger, J. Catal. 116 (1989) 31.
[8] H. Saitovitch, P.R.J. Silva, A.M. Rodriguez, J. Weberszpil, F.B. Passos, M. Schmal, Hyp. Int. 84 (1994) 563.
[9] F.B. Passos, P.R.J. Silva, H. Saitovitch, Stud. Surf. Sci. Catal. 130 (2000) 3195.
[10] G. Schatz, A. Weidinger, Nuclear Condensed Matter Physics: Nuclear Methods and Applications, Wiley, New York, 1996.
[11] G.L. Catchen, J. Mater. Educ. 12 (1990) 253.
[12] C.M. Lederer, J.M. Hollander, I. Perlman, Table of Isotopes, 6th ed., Wiley, New York, 1967.
[13] G.F. Knoll, Radiation Detection and Measurements, Wiley, New York, 1967.
[14] N. Wagstaff, R. Prins, J. Catal. 59 (1979) 563.
[15] H. Lieske, G. Lietz, H. Spindler, J. Völter, J. Catal. 81 (1983) 8.
[16] M. Uhrmacher, W. Bolse, Hyp. Int. 15–16 (1983) 4445.
[17] W. Bolse, M. Uhrmacher, K.P. Lieb, Mater. Sci. Eng. 69 (1985) 375.
[18] M. Marszalek, B. Wodniecki, P. Wodniecki, A.Z. Hrynkiewicz, Hyp. Int. 80 (1993) 1029.